

S2C2A: A Flexible Task Space Planning and Control Strategy for Modular Soft Robot Arms

Zixi Chen, Qinghua Guan, Josie Hughes, *Member, IEEE*, Arianna Menciassi, *Fellow, IEEE*, and Cesare Stefanini, *Member, IEEE*

Abstract—Modular soft robot arms (MSRAs) are composed of multiple independent modules connected in a sequence. Due to their modular structure and high degrees of freedom (DOFs), these modules can simultaneously bend at different angles in various directions, enabling complex deformation. This capability allows MSRAs to perform more intricate tasks than single-module robots. However, the modular structure also induces challenges in accurate planning, modeling, and control. Non-linearity, hysteresis, and gravity complicate the physical model, while the modular structure and increased DOFs further lead to accumulative errors along the sequence. To address these challenges, we propose a flexible task space planning and control strategy for MSRAs, named *S2C2A* (State to Configuration to Action). Our approach formulates an optimization problem, *S2C* (State to Configuration planning), which integrates various loss functions and a forward MSRA model to generate configuration trajectories based on target MSRA states. Given the model complexity, we leverage a biLSTM network as the forward model. Subsequently, a configuration controller *C2A* (Configuration to Action control) is implemented to follow the planned configuration trajectories, leveraging only inaccurate internal sensing feedback. Both a biLSTM network and a physical model are utilized for configuration control. We validated our strategy using a cable-driven MSRA, demonstrating its ability to perform diverse offline tasks such as position control, orientation control, and obstacle avoidance. Furthermore, our strategy endows MSRA with online interaction capability with targets and obstacles. Future work will focus on addressing MSRA challenges, such as developing more accurate physical models and reducing configuration estimation errors along the module sequence.

Index Terms—Planning, Control, Recurrent Neural Networks, Modular Soft Robot Arm

I. INTRODUCTION

IN comparison to rigid robots, soft robots have a number of advantages, with their most notable being their flexibility and compliance, which can provide safe yet robust environmental interactions. Due to this, they have been leveraged for

This work was supported by the European Union by the Next Generation EU project ECS00000017 ‘Ecosistema dell’Innovazione’ Tuscany Health Ecosystem (THE, PNRR, Spoke 4: Spoke 9: Robotics and Automation for Health.) Z. Chen and Q. Guan contributed equally to this work. *Corresponding authors: Zixi Chen

This work has been submitted to the IEEE for possible publication. Copyright may be transferred without notice, after which this version may no longer be accessible.

Zixi Chen, Arianna Menciassi, and Cesare Stefanini are with the Biorobotics Institute and the Department of Excellence in Robotics and AI, Scuola Superiore Sant’Anna, 56127 Pisa, Italy (e-mail: zixi.chen@santannapisa.it; arianna.menciassi@santannapisa.it; cesare.stefanini@santannapisa.it).

Qinghua Guan and Josie Hughes are with CREATE Lab, EPFL, Lausanne, Switzerland (e-mail: qinghua.guan@epfl.ch; josie.hughes@epfl.ch).

Digital Object Identifier (DOI): see top of this page.

various applications, including medical scenarios [1]–[3] and bionic robots [4]–[6]. Most soft robots are constructed from elastomeric materials [7], [8], incorporate deformable structures [9] or origami-inspired structure [10]. These materials and designs contribute to the lower stiffness and enhanced safety of soft robots compared to their traditional rigid counterparts. Resulting from their compliance, soft robots exhibit high degrees of freedom (DOFs) and, hence, are able to perform more diverse environmental interactions [11]. Consequently, soft robots have been successfully deployed in constrained working environments [12], such as the abdomen [13] and cluttered pipe environments [14].

Among the various categories of soft robots, modular soft robot arms (MSRA) have demonstrated significant potential, particularly due to their higher DOFs than single-module robots. Typically, one MSRA is composed of multiple independent modules connected in series, for example, as utilized by the robots described in [9], [15], [16], where modules are replicated to create a longer, more capable system [16], [17]. In most works, this kind of arm will be named as ‘soft continuum robot’ [18] or ‘soft continuum arm’ [19], but we use ‘modular soft robot arm’ to emphasize its modularity, which is the focus of this work. The presence of multiple modules increases the degrees of actuation within the same robot length, providing the robots with more diverse shape patterns [9] and a richer working space [16]. Due to these unique advantages, MSRAs have been leveraged in challenging tasks such as obstacle avoidance [20], rotating a handwheel, and opening a drawer [21].

Along with the high DOFs of MSRAs, their complex structures also pose challenges in accurate planning and control due to their softness and modularity. The inherent nonlinearity and hysteresis of the underlying structures make robot control a complex problem [22]. Furthermore, the modular structure complicates the mapping relationships among the task, configuration, and actuation spaces. As illustrated in Figure 1-(A), the module configurations will affect each other along the module sequence and ultimately determine the overall state of the soft robot, which infers that all configurations and their mutual influence should be considered in MSRA control. Such a requirement complicates the MSRA control issue compared to the single module arm control. Although physical model approaches have been widely employed in single module arm problems, the module improvement dramatically complicates the robot models [23], furthermore challenging the proposal of model-based controllers, specifically real-time ones.

Neural networks (NNs), particularly recurrent neural net-

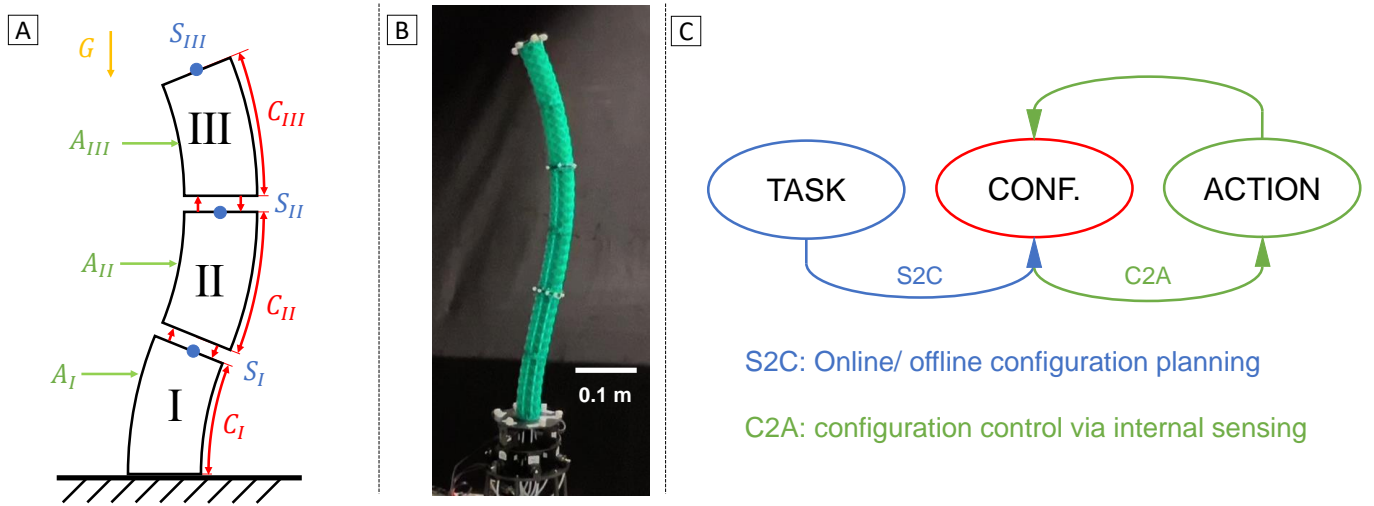


Fig. 1. (A) Modular soft robot arm motion diagram. The action of each module A_* (green) will directly affect the configurations C_* of each module (red) and indirectly affect the whole robot system state S_* (blue). The configurations of modules are affected by gravity and the adjacent modules. (B) MSRA applied in our experiments can deform in an S-shape, which single-module robots cannot achieve. (C) S2C2A comprises a configuration planning strategy S2C and a configuration controller C2A. S2C can propose the target configuration online or offline based on the task request. C2A collects configuration estimation from internal sensors and determines action based on the sensor feedback and target configuration from S2C.

works (RNNs), have been extensively leveraged in soft robot modeling and control. Due to the nonlinear activation functions, NNs are suitable for handling the nonlinear motions characteristic of soft robots [15]. Moreover, the recurrent structures of RNN can be employed to address sequence-related issues such as time delay [24] and MSRA configuration control [16]. As a result, RNNs have the potential to tackle the complexities posed by MSRAs.

This paper aims to propose a flexible MSRA task space planning and control strategy named S2C2A, as illustrated in Figure 1-(C). A configuration planning approach S2C is employed to generate configuration trajectories based on the task requirements online or offline using an optimization problem, and we apply a biLSTM network as the MSRA forward model in optimization. Additionally, a feedback configuration controller C2A specifically designed for MSRAs is employed to execute configuration control tasks, and both a biLSTM network and a physical controller are utilized. We validate our approach on a cable-driven MSRA, demonstrating its flexibility in achieving a variety of tasks.

The contributions of this paper are as follows:

- 1) We introduce a hierarchical MSRA task space planning and control strategy named S2C2A. The configuration trajectory is planned at first, and a configuration controller is used to control the configuration.
- 2) We utilize space sequence biLSTM serving as the MSRA forward model in the configuration planning optimization problem for online and offline planning.
- 3) We leverage both biLSTM and physical controller for configuration control even in the presence of inaccurate internal sensing feedback instead of external sensing.
- 4) Real experiments have been carried out to validate our strategy. Offline Tasks including position control, orientation control, and obstacle avoidance have been achieved successfully. Moreover, online interactions

with the target and obstacle are performed.

The remainder of the paper is structured as follows: Section II reviews works related to soft robot planning and control approaches, with a focus on MSRA. Section III describes the robot setup and the definitions of configuration and state. Section IV details the task space planning and control strategy S2C2A, covering configuration planning method S2C using biLSTM and configuration controller based on either biLSTM or a curvature model. Section V presents the real experimental results, which demonstrate that our controllers can perform a range of tasks, from basic ones like position and orientation control to more complex ones like obstacle avoidance and online target following. Section VI summarizes this paper and discusses potential directions for future work.

II. RELATED WORK

A. MSRA Planning

In robot planning, trajectories in the task or configuration space are calculated to achieve task requirements like trajectory following, orientation control, and obstacle avoidance. Effective planning is essential for high DOF robots like MSRA [25] and challenging working spaces like obstacle-included [26] and constrained environments [12]. Most studies about soft robot planning rely on physical models, and the constant curvature (CC) model [12] is the most popular one due to its simplicity and low computational cost. The shapes of the robot backbone, inflated chambers, and obstacles are considered in the planning strategy of [12] to propose available robot shapes for the MSRA. Similarly, the curvature model is also utilized in [27] in conjunction with rapidly exploring random trees for planning. To achieve inspection tasks in cluttered space, one MSRA is segmented into independent curvatures step by step to find feasible shapes in [14]. Additionally, a MSRA is represented by Bézier curves in [28] for planning.

In addition to physical models, some data-driven approaches are utilized. For instance, the Gaussian Mixture Model (GMM) is deployed in [25] to encode the spatial and temporal values from the human demonstration, and trajectory is generated through regression for MSRA. A 3D neural network is leveraged in [29] to reduce unnecessary sweeping motion in robot-assisted surgeries. The improved artificial potential field method is leveraged in [30] for an MSRA with five modules, where constraints and targets are integrated into loss functions of planning optimization. However, this optimization-based approach is only validated in simulation and with a single type of task. Similarly, optimization techniques are also employed in [31], [32], where the distances between the current state and the targets are defined as rewards, and those between the current state and the obstacles are defined as penalties.

It is challenging to build an accurate physical model for MSRAs, while data-driven approaches like NNs have limitations regarding task adaptability. Generally, a single NN is designed to handle a specific task, and it is difficult to adapt to varying or additional requirements with the same trained model. For instance, the NN controller in [33] aims to control robot position and orientation simultaneously. Utilizing such a controller, it is not possible to set only the position target without putting constraints on orientation, nor can the trained controller be easily extended to additional functions such as comprehensive shape control. Although optimization and NN forward model are also used in [24] for MSRA, it only achieves one kind of 2D trajectory following tasks and does not take full advantage of this optimization planning strategy. In this case, we leverage a biLSTM as a forward model within an optimization framework to enable flexible configuration planning. By modifying the cost function in the optimization problem, configuration trajectories tailored to different tasks can be determined.

B. Soft Robot Control

Based on proposed trajectories in the task or configuration space, a proper controller is essential to achieve trajectory following tasks. There have been several reviews focusing on soft robot control [22], [34]–[36]. Jacobian controllers have been applied in soft robots [37]. The Jacobian matrix is updated in real time, and the action is decided by either optimization problems [37] or the inverse Jacobian matrix [38]. Moreover, various categories of physical models, such as Piecewise Constant Curvature (PCC) [39]–[41], Cosserat rod [5], [42], [43], and Finite Element Methods (FEM) [44]–[46], have been leveraged for soft robot control. These methods aim to describe robot motion through physical deformation and design controllers based on these physical models.

In addition to the above physical controller, data-driven methods have also been applied to soft robot control. Statistical approaches such as support vector regressor (SVR) [47], Gaussian mixture model (GMM) [48], and Gaussian process regression (GPR) [3], [49] have been utilized. The soft robot motion is summarized by optimizing the parameters to propose the controllers. Currently, NNs are the most popular choice in this area. Considering the nonlinear activation functions,

NN controllers are suitable for soft robots exhibiting nonlinear behaviors. The research in soft robot NN control starts with simple NNs like extreme learning machine (ELM) [50], [51] and radial basis function (RBF) [52]–[54]. Multilayer perceptron (MLP) [55], [56] has been widely applied in soft robots, including sensing, modeling, and control. Due to the recurrent structure and soft robot hysteresis, RNNs are particularly well-suited for soft robot control [57], [58].

Although NN controllers have been extensively leveraged in many soft robot applications, they may not always address the specific physical requirements of these robots. For instance, the cable displacements in the cable-driven robots are not fully independent [59], and such coupling cannot be represented by the existing NN layers. Additionally, most works utilizing NN in MSRA employ external sensing systems like optical cameras, which are challenging to implement in real applications. In this work, we introduce an additional layer at the end of the biLSTM network to address the physical actuation requirements of the robot. In addition, we incorporate a CC controller to prove the flexibility of our proposed strategy. Configuration feedback is provided by only internal sensors, and the costly external sensing system is not necessary during control.

III. SETUP AND SPECIFICATION

A. Experimental Setup

In this paper, we utilized a cable-driven modular soft robot arm for our experiments, as shown in Figure 2-(A). The robot comprises three independent modules (about 0.2m for each module), and each module is actuated by three motors (DYNAMIXEL x1330-m077-t) fixed on the MSRA base via three cables placed at an interval angle of 120° along the circumferential direction. The cables of modules II and III pass through housing tubes, guaranteeing each module's independence. In other words, the actuation of cable III will only affect module III instead of the whole MSRA due to the housing tubes. More details of the robot setup, such as MSRA material and mechanical properties, can be found in [9].

For capturing a ground truth for the robot's position, several optical track markers are fixed at the end of each module and robot base. Six optical tracking cameras (Optitrack Prime 13) and motion capture software Motive (Optitrack) collect each module end positions and orientations for NN training and only monitoring during control. A laptop (Ubuntu 20.04, CPU i5-12500H, and GPU RTX 3050) receives optical tracking information from the Motive computer via an ethernet switch and communicates with motors via one u2d2 power hub board (DYNAMIXEL). All devices run at about 10Hz in data collection and control tasks.

B. State and Configuration

As shown in Figure 2-(B), we utilized the unit end orientation vector of each module subject to the module end (o_x, o_y, o_z) to represent module configuration C . We utilize it to describe module configuration following [16] rather than bending directions and angles because such a representation is more suitable for NN data training as the vector length has

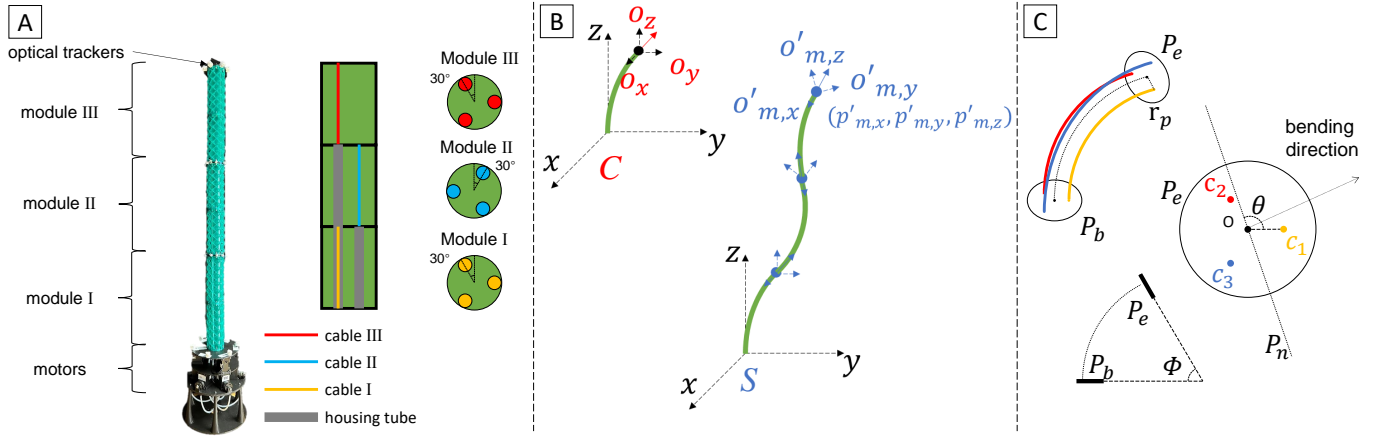


Fig. 2. (A) Robot setup. The cable-driven robot is composed of three independent segments, while each segment is actuated by three motors. The encoder in each motor provides feedback for configuration estimation. The optical tracking system is applied to provide ground truth robot states. (B) Configuration and state. Configurations (red) refer to segment end orientation relative to the segment base, and states (blue) refer to the position and orientation of every segment relative to the robot base. (C) Module actuation. The module configuration can be calculated by module bending angle ϕ and neutral surface direction θ , which can be estimated by the displacements of cables c_1, c_2, c_3 .

a fixed range and changes continuously. In contrast, bending direction angles experience abrupt changes from 360° to 0° when the orientation completes a full rotation, making them unsuitable for NN data training. The robot state S is composed of the position (p'_x, p'_y, p'_z) and orientation (o'_x, o'_y, o'_z) of every module end subject to the robot end. Therefore, module configurations are independent, and the configuration of one module will not affect those of the other modules. In contrast, the state of one module is affected by the states of base modules and its own configuration.

C. Configuration Estimation

To collect accurate MSRA states and configurations, most methods use an external sensing systems like the optical tracking system shown in Figure 2-(A) or electromagnetic tracking systems in [60] for accurate feedback control. However, such systems have strict requirements on optical or electromagnetic environments and are unsuitable for real applications like agriculture and domestic environments. In this work, we aim to perform MSRA state control only by employing internal sensing feedback. Encoders in the motors are employed in this work, and some other internal sensors such as IMU [61] and flex sensor [62] may also be utilized for replacing the encoder and providing internal sensing feedback in future work.

The encoder in the motor can measure cable displacement and serves as an internal module configuration sensor. Following [63], we estimate module orientation based on the cable displacement. Three cables c_1, c_2, c_3 are placed in each module, and O represents the plane center as shown in Figure 2-(C). In the initial state, the length of each cable and the module is l_0 . During the motion, we define the cable lengths as l_1, l_2, l_3 and the cable displacement $a_i = l_i - l_0$, where $i = 1, 2, 3$. Considering the low axial direction compressibility of each module, we assume that the module length does not change, and the displacements follow:

$$a_1 + a_2 + a_3 = 0. \quad (1)$$

To estimate the module configuration, first, we estimate the bending angle ϕ between the base plane P_b and the end plane P_e along with the angle θ between the neutral surface P_n and the $O - c_1$ axis by

$$\begin{aligned} \phi &= \frac{1}{r_p} \sqrt{a_1^2 + \frac{(a_2 - a_3)^2}{3}}, \\ \theta &= \text{atan2}(-a_1, \frac{a_2 - a_3}{\sqrt{3}}), \end{aligned} \quad (2)$$

where r_p represents the distance between the plane center and the cable position, as shown in Figure 2-(C). Then, the configuration (o_x, o_y, o_z) can be denoted as

$$\begin{aligned} o_x &= \sin(\phi) \cos(\theta - \frac{\pi}{2}), \\ o_y &= \sin(\phi) \sin(\theta - \frac{\pi}{2}), \\ o_z &= \cos(\phi). \end{aligned} \quad (3)$$

In this case, we can estimate the module configuration (o_x, o_y, o_z) based on encoder feedback a_1, a_2, a_3 .

D. Data Collection

Using the experiment devices mentioned in Sec. III-A, we collected 9000 data points, as depicted in Figure 3-(A) and (B), and the working space length of the MSRA end on the x, y , and z axis are about 0.99, 0.99, and 0.49 m. Instead of a purely random motor babbling strategy, we actuate the MSRA in different patterns, as illustrated in Figure 3-(C). All the modules are actuated with the same random action sequence a_I in the first one-third period. Then, in the second one-third period, the first and second modules are actuated with the same random action sequence a_I while the end module is actuated by a different action sequence a_{III} . In the final one-third period, all these modules are actuated by different random action sequences a_I, a_{II}, a_{III} . This data collection approach specifically for MSRAs is proposed in [16] and has demonstrated that it can explore a larger working space in the 3D space and varied module configuration combinations.

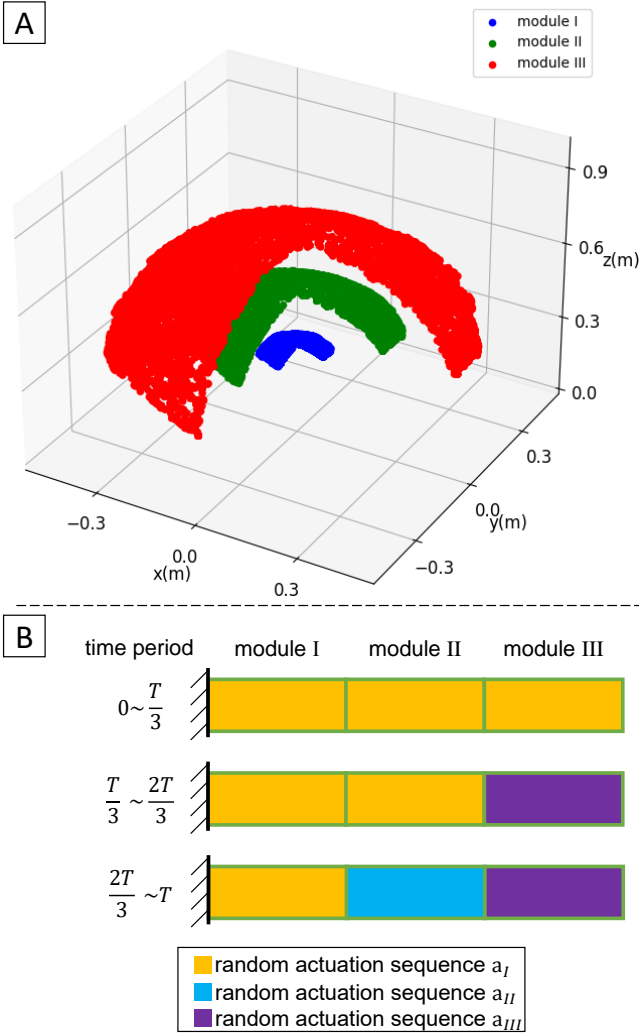


Fig. 3. (A) Some collected samples. Samples with $x > 0$ and $y < 0$ are hidden for visualization. The positions of the base module end, middle module end, and end module end are depicted as blue, green, and red dots. (B) Data collection strategy specifically for MSRAs.

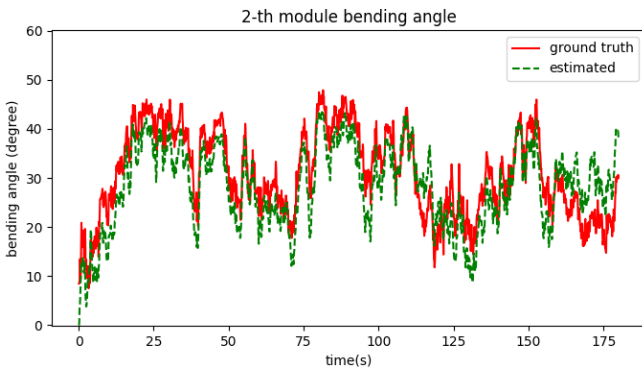


Fig. 4. The middle module bending angles estimated by the optical tracking system (ground truth, red) and encoders in motors (red).

We compare the real module configurations collected by the optical tracking system (ground truth) and the configurations estimated by encoder feedback following Equation 3. The estimation errors of the base, middle, and end modules are

7.02° , 8.07° , and 12.77° , respectively. An example of a comparison of the ground truth and estimated module bending angles during dynamic motion is shown in Figure 4. The increase in error along the module sequence could be attributed to gravity, hysteresis, and friction between the cables and modules. In this work, instead of using the optical tracking system as the configuration sensor, we aim to achieve state control even under the inaccurate configuration estimation. Such an implementation endows the MSRA with a tracking ability that relies only on internal sensing feedback instead of costly external sensing systems like optical and electromagnetic tracking systems. Internal sensing correction may be included in future work.

IV. PLANNING AND CONTROL METHODS

A. Configuration Planning - S2C

Our planning strategy is inspired by model predictive control (MPC), which determines action based on a forward model and an optimization problem. By adjusting the cost function in the optimization problem, diverse tasks can be performed. Considering the nonlinearity, hysteresis, and modularity of MSRAs, it is challenging to build an accurate physical model. Hence we leverage a biLSTM network NN_{C2S} as the forward model estimating state (\hat{p}', \hat{o}') based on module configuration C , as shown in Figure 5-(A). All the data, including robot states, configurations, and actions, are rescaled to $[-1, 1]$ for NN training. In this paper, we apply I, II, III to represent the module number and $1 \sim 5$ to represent the time step.

In order to fulfill various tasks, a series of losses is integrated into the cost function. To achieve position-tracking and orientation-tracking tasks, we introduce the losses

$$\begin{aligned} L_p &= \|p'_d - \hat{p}'\|_2, \\ L_o &= \|o'_d - \hat{o}'\|_2, \end{aligned} \quad (4)$$

where p'_d, o'_d are the desired state position and orientation from the target states.

To achieve obstacle avoidance, we define the loss

$$L_{ob} = \begin{cases} \frac{1}{d}, & d \leq r, \\ 0, & d > r, \end{cases} \quad (5)$$

where $d = \|p'_{ob} - \hat{p}'\|_2$ refers to the distance between the estimated position \hat{p}' and the obstacle center p'_{ob} . r defines the obstacle avoidance threshold according to the obstacle risk level.

Finally, we introduce a configuration change loss L_d to constrain the configuration change between two continuous steps.

$$L_d = \|\Delta C\|_2, \quad (6)$$

where $\Delta C = C - C_0$ denotes the difference between the last configuration C_0 and the next configuration C .

Overall, the configuration planning strategy can be illustrated as

$$\begin{aligned} \min_C & \mu_p L_p + \mu_o L_o + \mu_{ob} L_{ob} + \mu_d L_d, \\ \text{s.t.} & (\hat{p}', \hat{o}') = NN_{C2S}(C) \end{aligned} \quad (7)$$

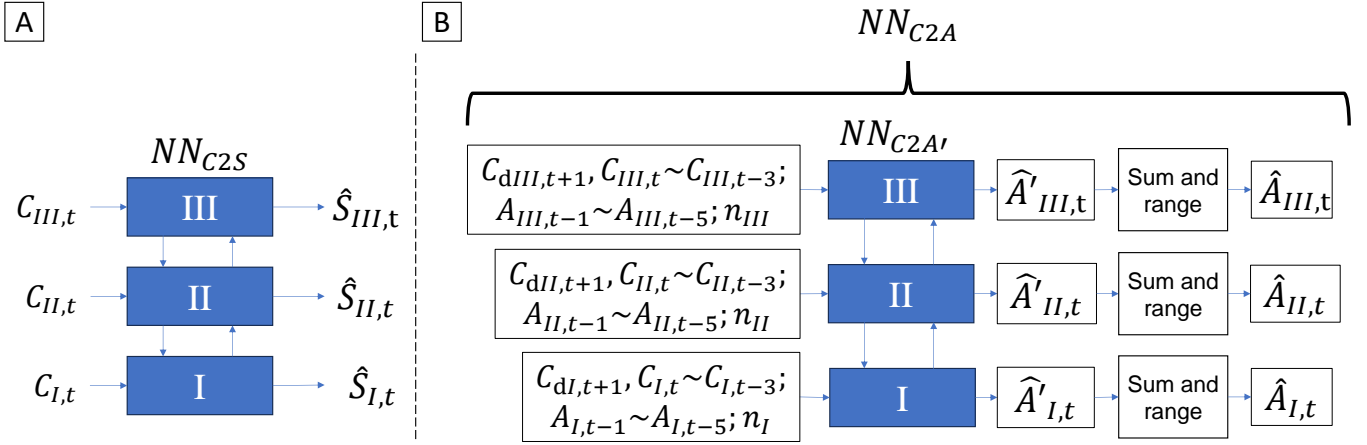


Fig. 5. (A) Space sequence biLSTM network NN_{C2S} . Each biLSTM unit takes configurations C_* of one module as input to estimate the robot states \hat{S}_* . (B) Configuration Controller NN_{C2A} . A biLSTM network $NN_{C2A'}$ decides the action $\hat{A}_{*,t}$ based on the previous actions $A_{*,t-1} \sim A_{*,t-5}$, target and previous states $C_{d*,t+1}$, $C_{*,t} \sim C_{*,t-3}$, and module labels n_* . The 'sum and range' layer is applied to guarantee the actuation sum and range.

where $\mu_p, \mu_o, \mu_{ob}, \mu_d$ represent the weights of position control, orientation control, obstacle avoidance, and configuration change. NN_{C2S} serves as a forward model estimating the robot state (\hat{p}', \hat{o}') from the module configurations C , and the module configurations C are optimized to minimize the cost function.

Compared to other NN implementations in soft robots which only target a single task, such a planning strategy is adaptive to various tasks. Moreover, this planning strategy can be implemented both offline and online, depending on the task requirements.

B. Configuration Control - C2A

Following [16], we utilize a biLSTM $NN_{C2A'}$ and a 'sum and range' layer to compose NN_{C2A} as the configuration controller for MSRAs, as shown in Figure 5-(B). The controller can be represented as

$$\hat{A}_t = NN_{C2A}(C_{d,t+1}; C_t \sim C_{t-3}; A_{t-1} \sim A_{t-5}; n), \quad (8)$$

where NN_{C2A} illustrates the controller that determines the t step action \hat{A}_t based on the target configuration $C_{d,t+1}$, previous configurations $C_t \sim C_{t-3}$, previous actions $A_{t-1} \sim A_{t-5}$, and module label n .

The module label $n_m \in [-1, 1]$ of the m -th module is utilized to infer the module position in the module sequence, which can be presented as

$$n_m = \frac{2(m-1)}{n_{sum}-1} - 1, \quad (9)$$

where n_{sum} denotes the amount of modules in the MSRA. A higher label represents that the module is near the MSRA end rather than the base.

The actions of each module $\hat{A}_{m,t} \in R^3$ should follow the constraint in Equation 1 and in the range $[-1, 1]$. Hence, one layer follows the biLSTM

$$\hat{A}_{m,t} = \frac{3 \tanh(A_{m,t}^{\hat{}}) - \sum \tanh(A_{m,t}^{\hat{}})}{4}, \quad (10)$$

where $A_{m,t}^{\hat{}}$ represents the biLSTM $NN_{C2A'}$ output of the m -th module at t -th step.

Considering the uniform deformation of our cable-driven robots, a physical controller based on the CC model can also be applied for configuration control. To decide the action $\hat{a}_1, \hat{a}_2, \hat{a}_3$ based on the desired configuration (o_{dx}, o_{dy}, o_{dz}) , we first calculate the desired bending angle ϕ_d and neutral surface direction θ_d by

$$\begin{aligned} \theta_d &= \text{atan2}(o_{dy}, o_{dx}) + \frac{\pi}{2}, \\ \phi_d &= \text{atan2}\left(\frac{o_{dy}}{\sin(\theta_d - \frac{\pi}{2})}, o_{dz}\right). \end{aligned} \quad (11)$$

Then, we decide the actions by

$$\begin{aligned} \hat{a}_1 &= -\phi_d r_p \sin(\theta_d), \\ \hat{a}_2 &= \phi_d r_p \sin\left(\frac{2\pi}{3} - \theta_d\right), \\ \hat{a}_3 &= \phi_d r_p \sin\left(\theta_d - \frac{\pi}{3}\right). \end{aligned} \quad (12)$$

Compared to the physical controller, the data-driven controller NN_{C2A} is a more general controller available for various soft robots, like the pneumatic MSRA in [16] and the cable-driven MSRA in this work. However, this physical controller is only available to the soft robots following the CC assumption. Different modules require specific physical models and the targeted controller, but physical approaches have higher explainability than the black-box NN controller. Overall, the S2C2A strategy can implement different configuration controllers based on the MSRA properties and task requirements.

Utilizing the dataset collected in Section III-D, we train NN_{C2S} and NN_{C2A} for configuration planning and control, and the NN hyperparameters are shown in Table I. Of note, the configuration applied in NN training is only from internal sensors, not the optical system. NN_{C2A} contains fewer layers and a smaller hidden state size to decrease the online computation burden.

To minimize the cost functions in Equation 7 and generate the target configuration online or offline, we employ Pytorch

TABLE I
NN HYPERPARAMETERS

| | NN_{C2S} | NN_{C2A} |
|--------------------------|-------------------|-------------------|
| layer number | 4 | 2 |
| time step | / | 5 |
| hidden state size | 64 | 32 |
| learning rate | 0.001 | 0.001 |
| batch size | 64 | 64 |
| optimizer | Adma | Adam |
| average estimation error | $1.36 \pm 1.21\%$ | $1.07 \pm 1.89\%$ |

[64], and the optimizer is Adam. The learning rate is 0.02, and the optimization iteration is 10.

V. EXPERIMENTAL RESULTS

A. Position Control

We propose a position trajectory in the task space, as shown in the red lines in Figure 6, and employ our approach to achieve position control. Following the target trajectory, the MSRA will first bend along the x-axis and rotate to move along a circle. We include the losses L_p and L_d for position tracking and compare the performance of NN_{C2A} and the physical CC controller. In this task, $u_p = 1$ and $u_d = 0.5$. The errors of trajectories using NN controller and CC controller are shown in Table II. The MSRA trajectories and robot motions are shown in Figure 6 and 7. All the experiment videos can be found in the Supplementary Video.

TABLE II
ERRORS AND STANDARD DERIVATIONS IN POSITION CONTROL

| C2A | position error |
|------|------------------|
| NN | 2.8 ± 1.0 cm |
| CC | 3.7 ± 1.4 cm |

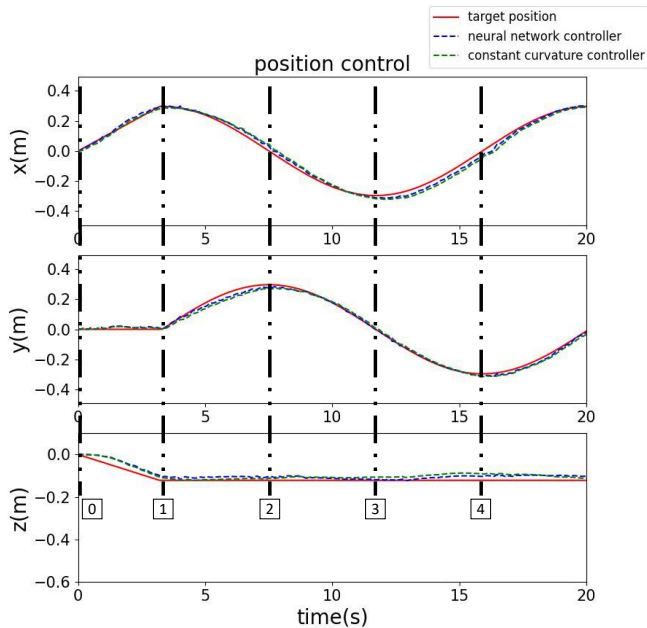


Fig. 6. The target (red) trajectories in the position control task and real trajectories applying NN_{C2A} (blue) and CC controller (green).

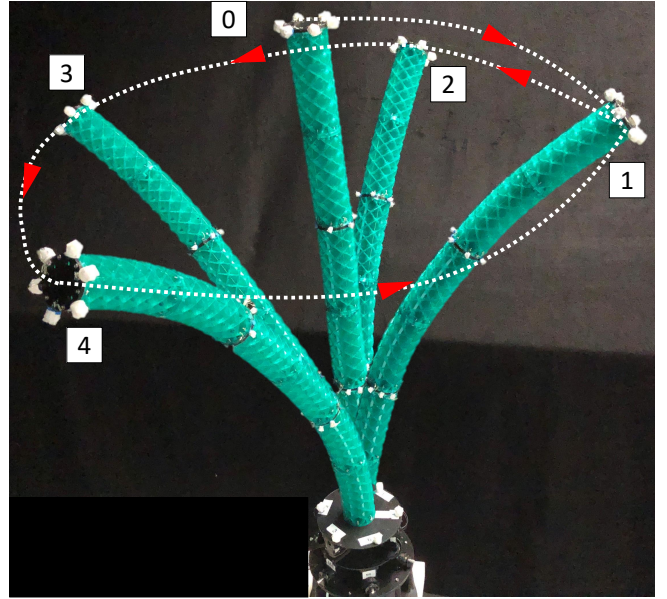


Fig. 7. The MSRA motion in position control using the configuration controller NN_{C2A} . The MSRA first decreases the height (1-2) and draws a circle (2-3-4-5). The white dotted lines represent the MSRA end trajectories, and the red arrows represent the motion directions.

Of note, the MSRA states collected by the optical tracking system are only used for comparing with the target trajectory, and we do not utilize them as feedback in the following experiments, which is proven obviously in Section V-E. Only encoder feedback is fed into the configuration controller. The experimental results show that the configuration controller NN_{C2A} outperforms the CC controller; hence, we employ it in the following experiments.

B. Position and Orientation Control

In addition to the position trajectory shown in Figure 6, we add target angle trajectories for MSRA end orientation, as depicted in the red lines in Figure 9. In these tasks, we include the losses L_p , L_d and the orientation loss L_o for tracking. First, we define three tasks requiring the bending angle to 40° , 50° , and 60° , as shown in Figure 10-(A), (B), and (C). In the fourth task, the MSRA is controlled to keep the end upward while following a circle, as illustrated in Figure 10-(D). In these tasks, $u_p = 1$, $u_d = 0.5$, and $u_o = 2$. The errors are shown in Table III. All the experiment videos can be found in the Supplementary Video.

TABLE III
ERRORS AND STANDARD DERIVATIONS IN POSITION AND ORIENTATION CONTROL

| task | position error | orientation error (z) | orientation error (x) |
|-----------------------|------------------|-----------------------|-----------------------|
| 40° | 3.9 ± 1.6 cm | $3.1 \pm 3.7^\circ$ | / |
| 50° | 3.2 ± 1.3 cm | $3.9 \pm 3.9^\circ$ | / |
| 60° | 3.1 ± 1.5 cm | $2.8 \pm 3.3^\circ$ | / |
| 0° | 2.7 ± 1.1 cm | $4.3 \pm 2.6^\circ$ | / |
| $50^\circ a 20^\circ$ | 3.4 ± 2.0 cm | $1.7 \pm 1.9^\circ$ | $4.5 \pm 4.9^\circ$ |
| $50^\circ c 20^\circ$ | 3.4 ± 1.6 cm | $3.9 \pm 3.2^\circ$ | $6.0 \pm 4.9^\circ$ |

Based on the task 50° , we also control the MSRA to bend 20° anticlockwise ($50^\circ a 20^\circ$) and clockwise ($50^\circ c 20^\circ$) on the

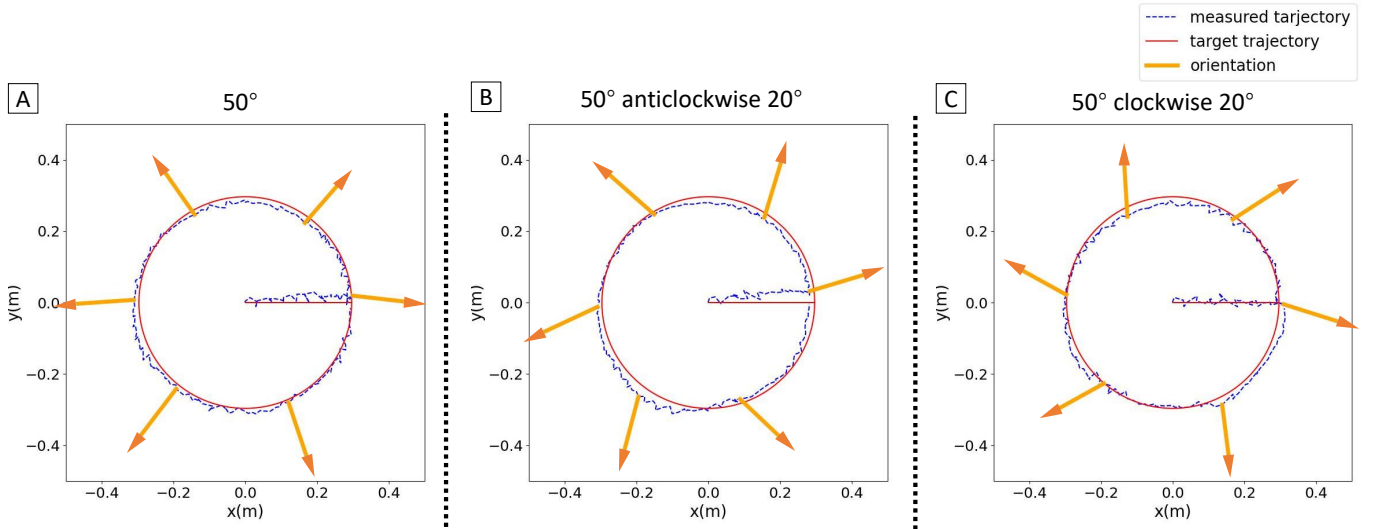


Fig. 8. The target (red) and real (blue) MSRA end motion on the x-y plane for the task (A) 50° , (B) $50^\circ a20^\circ$, (C) $50^\circ c20^\circ$. The yellow lines depict the end orientations on the x-y plane.

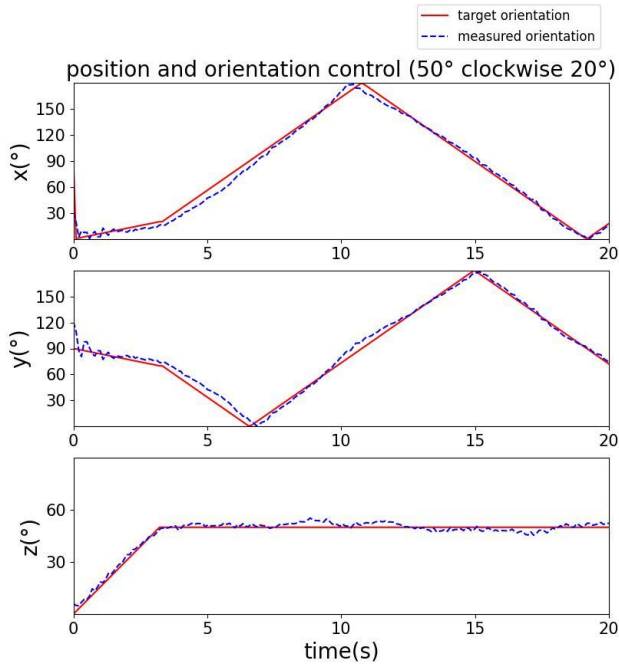


Fig. 9. The target (red) and real (blue) orientation trajectories in the position and orientation control task for 50° .

x-y plane. The errors are shown in Table III. We show the MSRA deformation on the same end position in Figure 10-(E), (F), and (G). The MSRA orientations on the x-y plane in these tasks are shown in Figure 8. It is obvious that our approach can perform position and orientation control simultaneously and achieve satisfying accuracy even in some intricate tasks.

C. Position Constraint

In these tasks, we aim to keep the end position of the base, middle, and end module invariant during motion, as depicted in Figure 11. We include the losses L_p, L_d, L_o for this task.

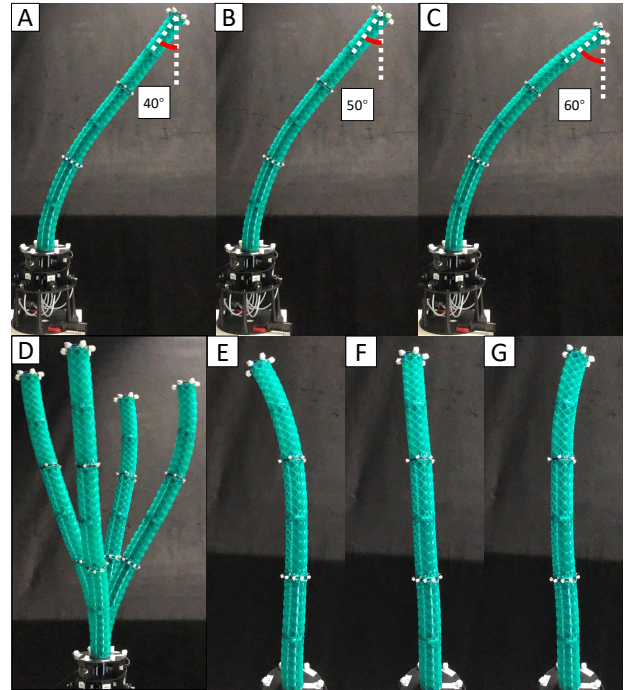


Fig. 10. The MSRA motion for (A) 40° , (B) 50° , (C) 60° , (D) 0° in position and orientation control. MSRA motion comparison for the task (E) $50^\circ a20^\circ$, (F) 50° , and (G) $50^\circ c20^\circ$.

In task 'base,' we control the MSRA end to follow a position trajectory while maintaining the base module position static, as shown in Figure 11-(A). In tasks 'middle' and 'end,' we aim to keep the middle and end module end positions static and change the same module end orientations, as shown in Figure 11-(B) and (C). The errors are shown in Table IV. During these motions, the corresponding module end positions remain static, but the orientations keep changing for MSRA motion. All the experiment videos can be found in the Supplementary Video.

TABLE IV
ERRORS AND STANDARD DERIVATIONS IN POSITION CONSTRAINT

| task | constraint error | motion error |
|--------|------------------|---------------------|
| base | 0.1 ± 0.1 cm | 3.1 ± 1.0 cm |
| middle | 3.0 ± 1.2 cm | $3.9 \pm 2.0^\circ$ |
| end | 5.3 ± 1.4 cm | $3.8 \pm 2.3^\circ$ |

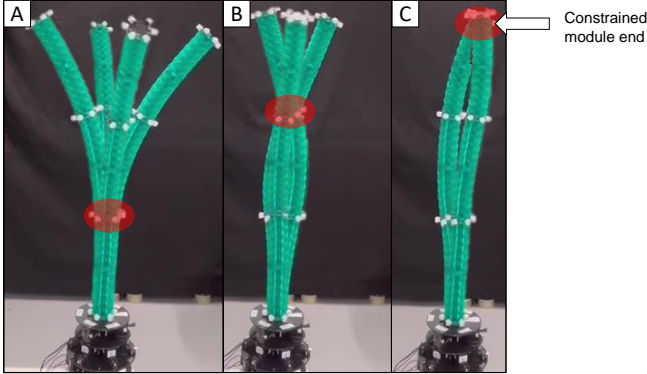


Fig. 11. The MSRA motion for the task (A) base, (B) middle, and (C) end in position constraint control. The red transparent circles depict the module end that remains its position.

D. Obstacle Avoidance

In obstacle avoidance, we include the losses L_p, L_d for position control and leverage the obstacle loss L_{ob} . First, we set a red sponge bar as the target and control the MSRA end to reach it, as illustrated in Figure 12-(A). Then, we put one blue sponge bar as the obstacle in the last MSRA end trajectory and include L_{ob} for replanning ($u_{ob} = 1$). The MSRA end first moves away from the obstacle to avoid collision (Figure 12-(B2)) and then reaches the target (Figure 12-(B3)). Furthermore, we set one more obstacle in the last MSRA end trajectory as depicted in Figure 12-(C). In this case, the S2C planning approach changes the trajectory and helps the MSRA reach the target.

By adjusting the obstacle threshold r mentioned in Equation 5, the MSRA will try to escape the obstacle when it enters the obstacle areas with different sizes. In this case, the obstacles can have different 'risk levels.' As shown in Figure 13, two obstacles are in the way of the MSRA end to the target. If both obstacles are at the high-risk level, which means the obstacle threshold is large, the MSRA will vibrate near the obstacle boundaries instead of taking risks and rushing to the target, as shown in Figure 13-(B). However, if one obstacle is at low risk, like the left one in Figure 13-(A) and the right one in Figure 13-(C), S2C will generate available trajectories reaching the target and the MSRA end will move to the target. The trajectories will be away from the high-risk obstacles and near the low-risk ones. All the experiment videos can be found in the Supplementary Video.

E. Online Interaction

If the obstacle and target will move during the task, it is necessary to plan the trajectory online. We include the losses L_p, L_d, L_{ob} for position control and obstacle avoidance in this task. During the motion, we cover the optical tracker markers

with a red cloth to highlight that we achieve accurate control via only motor encoder feedback. As shown in Figure 14-(A), a blue obstacle is moved to reach the MSRA end by hand, and the MSRA end will leave the obstacle as long as it is inside the obstacle area, whose size depends on the obstacle threshold r . In addition to online obstacle avoidance, target following can also be fulfilled online. In Figure 14-(B), the MSRA end will follow the moving target. The MSRA end will stop if the target is out of the working space, but it will start to reach the target again if the target reenters the working space, as shown in Figure 14-(C). All the experiment videos can be found in the Supplementary Video.

The online target following motion is steady because the MSRA always aims to minimize the distance between the target and MSRA, which is motivated by the loss L_p . Meanwhile, in online obstacle avoidance, the MSRA motion is discontinuous. When the obstacle moves near the MSRA and their distance is smaller than r in Equation 5, the MSRA will start to move away from the obstacle until the distance is larger than r . At this time, the MSRA will stop because of the configuration change loss L_d preventing unnecessary motion, which leads to such discontinuous motion. MSRA will start to move when the obstacle catches the MSRA end again. The obstacle threshold r constraints the obstacle avoidance L_{ob} into a local area, hence the loss will only take effect when the MSRA is within the 'risk area,' as the bordered blue circles in Figure 13 and 14. Therefore, we endow the MSRA with situation awareness to some extent, which may be significant in the interaction tasks in future work.

VI. CONCLUSION AND DISCUSSION

This work proposes a task space planning and control strategy S2C2A specifically for MSRAs that is flexible to tasks and controllers. We train a biLSTM network NN_{C2S} mapping from configuration to task space as the MSRA forward model and leverage it in an optimization problem S2C for configuration planning. Then, we train a biLSTM network NN_{C2A} for configuration control C2A and compare it with a physical CC controller. Utilizing a cable-driven MSRA, we demonstrate that our approach can achieve simple tasks like position control. Furthermore, some challenging tasks have been managed, such as position and orientation control, obstacle avoidance, and online planning. All the tasks can be achieved with low errors ($< 4\%$ in position and $< 5^\circ$ in orientation).

This flexible planning and control strategy endows MSRAs with accurate and complex deformation capability. Owing to modularity, MSRAs have the potential to perform sophisticated tasks, but effective control approaches specifically for MSRAs have not been fully explored. This work is a benchmark for MSRA control targeted at complicated deformation, enabling MSRA with flexibility and situation awareness. For instance, MSRAs can be utilized for minimally invasive surgery leveraging the position constraint ability and human interaction leveraging online planning ability.

We plan to design better controllers based on S2C2A in future work. For example, internal sensing errors will accumulate along the module sequence. More accurate configuration

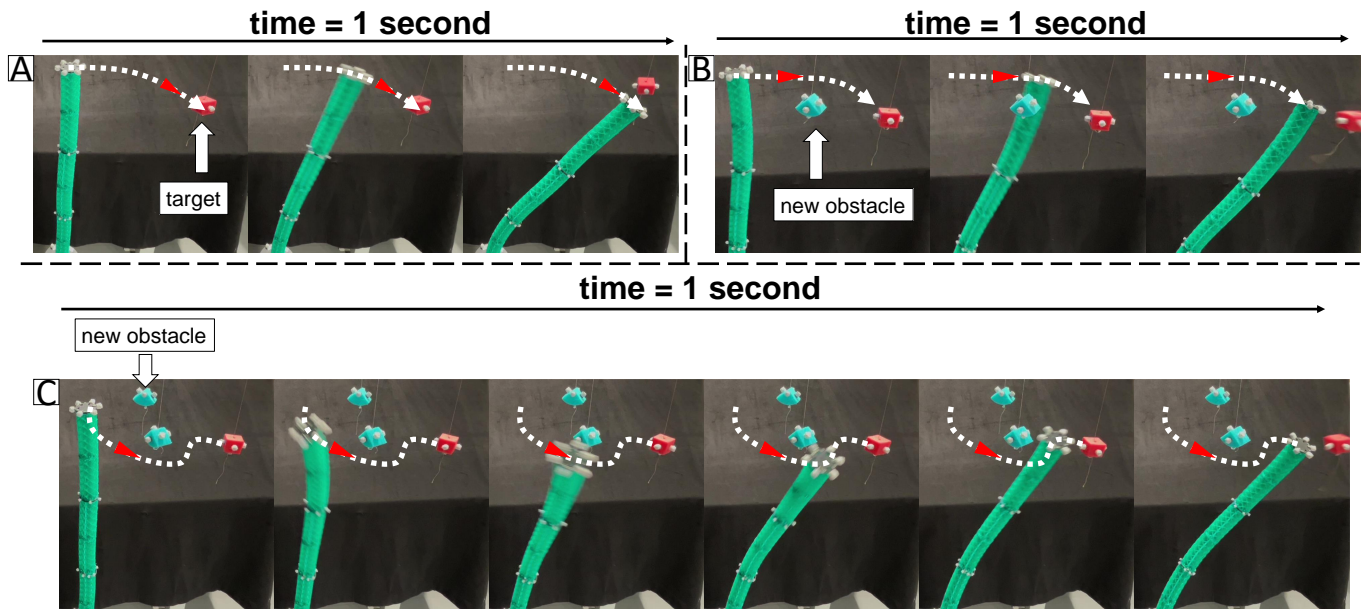


Fig. 12. The MSRA motion for the task in obstacle avoidance control with (A) 0, (B) 1, and (C) 2 obstacles. The white dotted lines represent the MSRA end trajectories, and the red arrows represent the motion directions. Red and blue sponge cubes represent the target and obstacles.

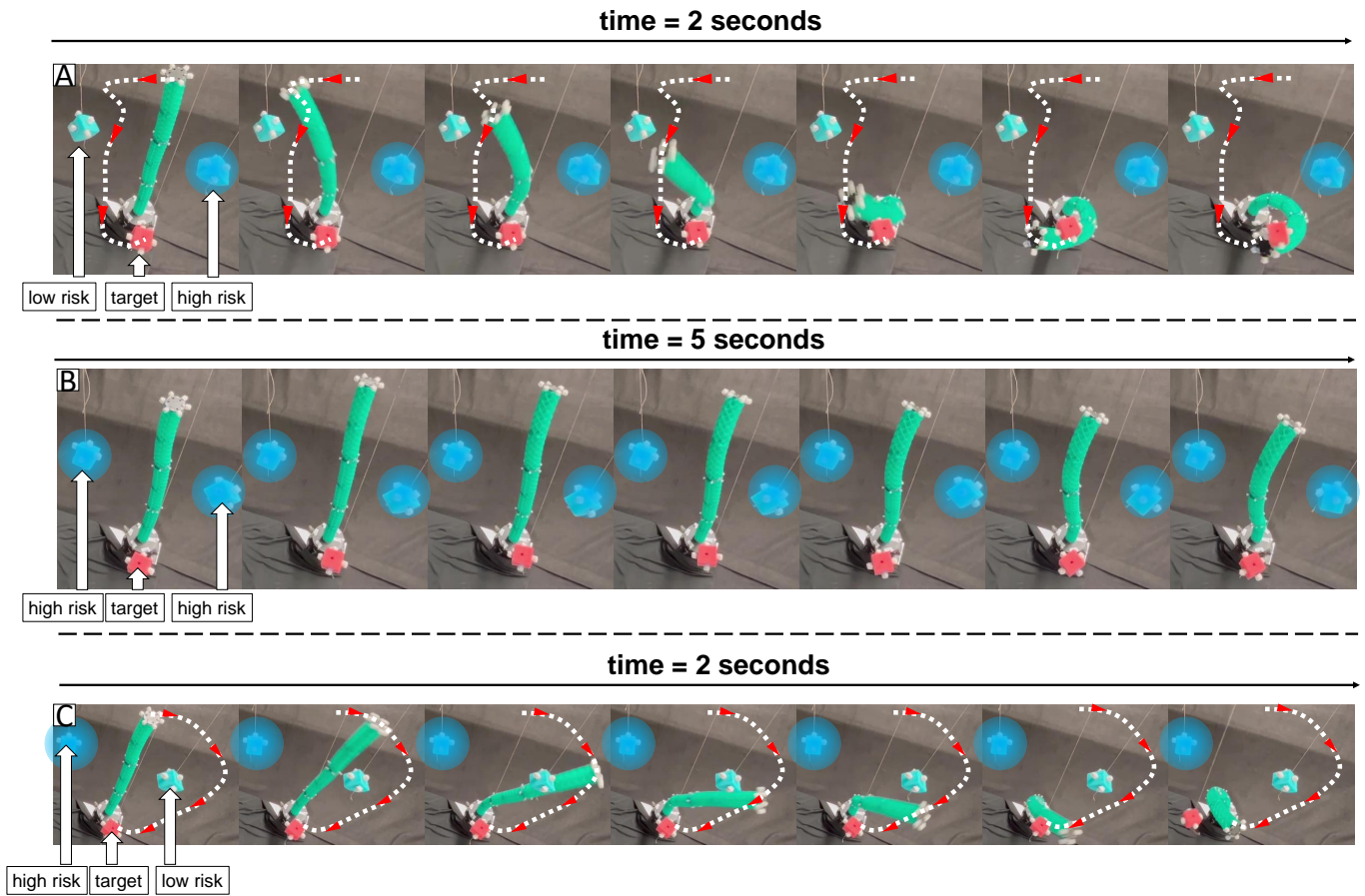


Fig. 13. The MSRA motion for the task in obstacle avoidance control with different obstacle thresholds. Red and blue sponge cubes represent the target and obstacles. The blue transparent circles represent the high risk areas. The white dotted lines represent the MSRA end trajectories, and the red arrows represent the motion directions. Red and blue sponge cubes represent the target and obstacles.

feedback may be possible by using IMU [61] and flex sensor [62]. It is challenging to estimate whether one target position

is feasible for one MSRA, and the difficulty will increase when including target orientation additionally. A novel controller

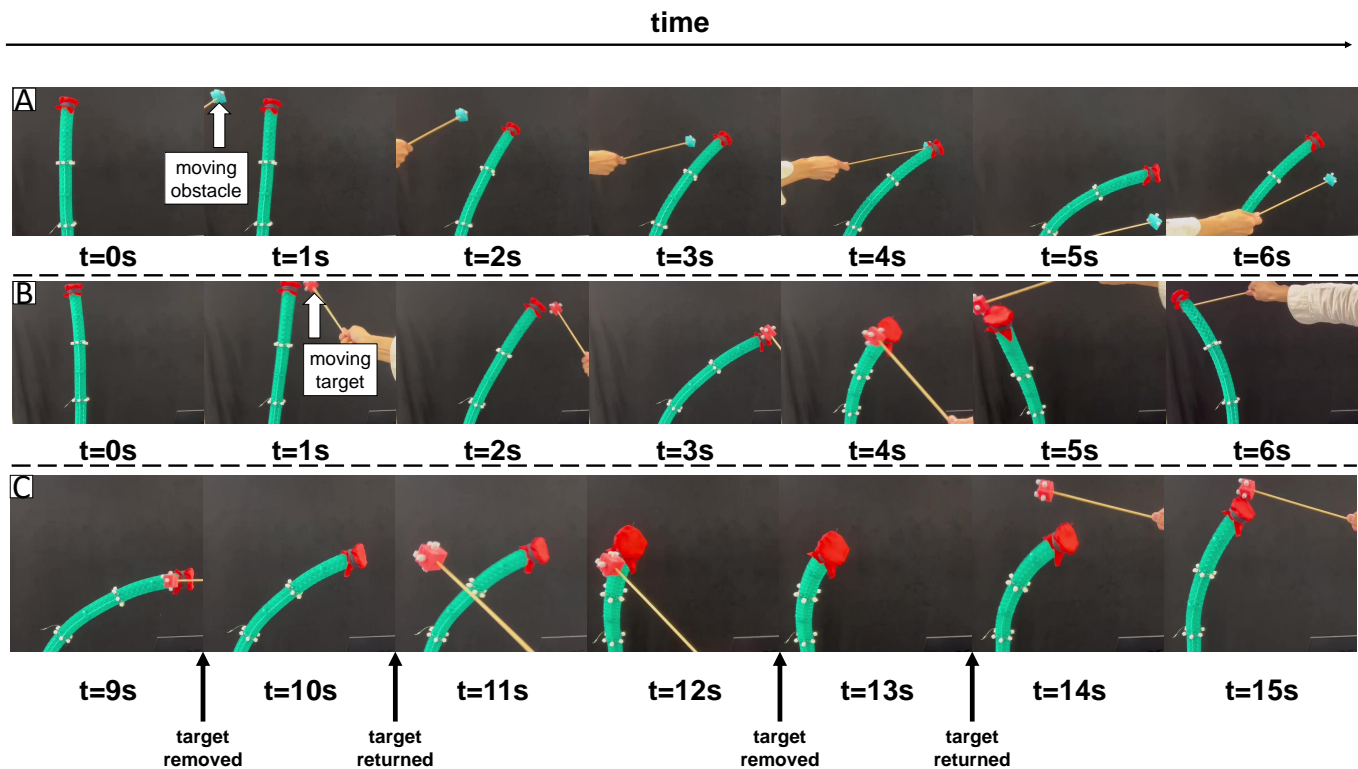


Fig. 14. Online planning motion for (A) obstacle avoidance and (B) target following. (C) The MSRA can reach the target even if it leaves and reenters the working space.

is required to achieve whole shape control, not only just module end state control. Moreover, we would like to take full advantage of the situation awareness ability equipped by our strategy and perform some more intricate interaction tasks.

REFERENCES

- [1] M. Cianchetti, T. Ranzani, G. Gerboni, I. De Falco, C. Laschi, and A. Menciassi, "Stiff-flop surgical manipulator: Mechanical design and experimental characterization of the single module," in *2013 IEEE/RSJ international conference on intelligent robots and systems*. IEEE, 2013, pp. 3576–3581.
- [2] M. Cianchetti, C. Laschi, A. Menciassi, and P. Dario, "Biomedical applications of soft robotics," *Nature Reviews Materials*, vol. 3, no. 6, pp. 143–153, 2018.
- [3] Z. Q. Tang, H. L. Heung, X. Q. Shi, K. Y. Tong, and Z. Li, "Probabilistic model-based learning control of a soft pneumatic glove for hand rehabilitation," *IEEE Transactions on Biomedical Engineering*, vol. 69, no. 2, pp. 1016–1028, 2021.
- [4] S. Mao, E. Dong, H. Jin, M. Xu, S. Zhang, J. Yang, and K. H. Low, "Gait study and pattern generation of a starfish-like soft robot with flexible rays actuated by smas," *Journal of Bionic Engineering*, vol. 11, no. 3, pp. 400–411, 2014.
- [5] F. Renda, M. Giorelli, M. Calisti, M. Cianchetti, and C. Laschi, "Dynamic model of a multibending soft robot arm driven by cables," *IEEE Transactions on Robotics*, vol. 30, no. 5, pp. 1109–1122, 2014.
- [6] Q. Guan, J. Sun, Y. Liu, N. M. Wereley, and J. Leng, "Novel bending and helical extensile/contractile pneumatic artificial muscles inspired by elephant trunk," *Soft robotics*, vol. 7, no. 5, pp. 597–614, 2020.
- [7] C. Laschi, M. Cianchetti, B. Mazzolai, L. Margheri, M. Follador, and P. Dario, "Soft robot arm inspired by the octopus," *Advanced robotics*, vol. 26, no. 7, pp. 709–727, 2012.
- [8] X. Ren, Y. Huan, M. Finocchiaro, M. Cianchetti, G. L. Secco, S. Wang, P. Dario, A. Koulaouzidis, A. Arezzo, and G. Ciuti, "Soft robotic gastroscope for low/middle-income countries: Design and preliminary validation," *IEEE Transactions on Medical Robotics and Bionics*, 2024.
- [9] Q. Guan, F. Stella, C. Della Santina, J. Leng, and J. Hughes, "Trimmed helicoids: an architected soft structure yielding soft robots with high precision, large workspace, and compliant interactions," *npj Robotics*, vol. 1, no. 1, p. 4, 2023.
- [10] M. Salerno, K. Zhang, A. Menciassi, and J. S. Dai, "A novel 4-dof origami grasper with an sma-actuation system for minimally invasive surgery," *IEEE Transactions on Robotics*, vol. 32, no. 3, pp. 484–498, 2016.
- [11] J. Jørgensen, K. B. Bojesen, and E. Jochum, "Is a soft robot more 'natural'? exploring the perception of soft robotics in human–robot interaction," *International Journal of Social Robotics*, vol. 14, no. 1, pp. 95–113, 2022.
- [12] A. D. Marchese, R. K. Katzschmann, and D. Rus, "Whole arm planning for a soft and highly compliant 2d robotic manipulator," in *2014 IEEE/RSJ International Conference on Intelligent Robots and Systems*. IEEE, 2014, pp. 554–560.
- [13] M. Cianchetti, T. Ranzani, G. Gerboni, T. Nanayakkara, K. Althoefer, P. Dasgupta, and A. Menciassi, "Soft robotics technologies to address shortcomings in today's minimally invasive surgery: the stiff-flop approach," *Soft robotics*, vol. 1, no. 2, pp. 122–131, 2014.
- [14] J. Li and J. Xiao, "Task-constrained continuum manipulation in cluttered space," in *2014 IEEE International Conference on Robotics and Automation (ICRA)*. IEEE, 2014, pp. 2183–2188.
- [15] T. G. Thuruthel, E. Falotico, M. Cianchetti, and C. Laschi, "Learning global inverse kinematics solutions for a continuum robot," in *ROMANSY 21-Robot Design, Dynamics and Control: Proceedings of the 21st CISM-IFTOMM Symposium, June 20-23, Udine, Italy*. Springer, 2016, pp. 47–54.
- [16] Z. Chen, M. Bernabei, V. Mainardi, X. Ren, G. Ciuti, and C. Stefanini, "A novel and accurate lstm configuration controller for modular soft robots with module number adaptability," *arXiv preprint arXiv:2401.10997*, 2024.
- [17] C. Della Santina, R. L. Truby, and D. Rus, "Data-driven disturbance observers for estimating external forces on soft robots," *IEEE Robotics and automation letters*, vol. 5, no. 4, pp. 5717–5724, 2020.
- [18] J. D. Greer, T. K. Morimoto, A. M. Okamura, and E. W. Hawkes, "Series pneumatic artificial muscles (spams) and application to a soft continuum robot," in *2017 IEEE International Conference on Robotics and Automation (ICRA)*. IEEE, 2017, pp. 5503–5510.

- [19] Y. Toshimitsu, K. W. Wong, T. Buchner, and R. Katzschmann, "Sopra: Fabrication & dynamical modeling of a scalable soft continuum robotic arm with integrated proprioceptive sensing," in *2021 IEEE/RSJ International Conference on Intelligent Robots and Systems (IROS)*. IEEE, 2021, pp. 653–660.
- [20] M. S. Nazeer, C. Laschi, and E. Falotico, "RI-based adaptive controller for high precision reaching in a soft robot arm," *IEEE Transactions on Robotics*, 2024.
- [21] H. Jiang, Z. Wang, Y. Jin, X. Chen, P. Li, Y. Gan, S. Lin, and X. Chen, "Hierarchical control of soft manipulators towards unstructured interactions," *The International Journal of Robotics Research*, vol. 40, no. 1, pp. 411–434, 2021.
- [22] T. George Thuruthel, Y. Ansari, E. Falotico, and C. Laschi, "Control strategies for soft robotic manipulators: A survey," *Soft robotics*, vol. 5, no. 2, pp. 149–163, 2018.
- [23] Y. Li, D. H. Myszka, and A. Murray, "The kinematics of constant curvature continuum robots through three segments," *IEEE Robotics and Automation Letters*, vol. 8, no. 11, pp. 7631–7638, 2023.
- [24] T. G. Thuruthel, E. Falotico, M. Manti, and C. Laschi, "Stable open loop control of soft robotic manipulators," *IEEE Robotics and Automation Letters*, vol. 3, no. 2, pp. 1292–1298, 2018.
- [25] H. Wang, J. Chen, H. Y. Lau, and H. Ren, "Motion planning based on learning from demonstration for multiple-segment flexible soft robots actuated by electroactive polymers," *IEEE Robotics and Automation Letters*, vol. 1, no. 1, pp. 391–398, 2016.
- [26] B. Ouyang, Y. Liu, H.-Y. Tam, and D. Sun, "Design of an interactive control system for a multisection continuum robot," *IEEE/ASME Transactions on Mechatronics*, vol. 23, no. 5, pp. 2379–2389, 2018.
- [27] B. H. Meng, I. S. Godage, and I. Kanj, "Rrt*-based path planning for continuum arms," *IEEE Robotics and Automation Letters*, vol. 7, no. 3, pp. 6830–6837, 2022.
- [28] Z. Mu, Y. Chen, Z. Li, C. Wang, N. Ding, and H. Qian, "A combined planning method based on biarc curve and bézier curve for concentric cable-driven manipulators working in confined environments," *IEEE/ASME Transactions on Mechatronics*, vol. 27, no. 6, pp. 4475–4486, 2022.
- [29] Y. Chen, W. Xu, Z. Li, S. Song, C. M. Lim, Y. Wang, and H. Ren, "Safety-enhanced motion planning for flexible surgical manipulator using neural dynamics," *IEEE Transactions on Control Systems Technology*, vol. 25, no. 5, pp. 1711–1723, 2016.
- [30] Y. Tian, X. Zhu, D. Meng, X. Wang, and B. Liang, "An overall configuration planning method of continuum hyper-redundant manipulators based on improved artificial potential field method," *IEEE Robotics and Automation Letters*, vol. 6, no. 3, pp. 4867–4874, 2021.
- [31] J. Lai, B. Lu, Q. Zhao, and H. K. Chu, "Constrained motion planning of a cable-driven soft robot with compressible curvature modeling," *IEEE robotics and automation letters*, vol. 7, no. 2, pp. 4813–4820, 2022.
- [32] M. Ding, X. Zheng, L. Liu, J. Guo, and Y. Guo, "Collision-free path planning for cable-driven continuum robot based on improved artificial potential field," *Robotica*, pp. 1–18, 2024.
- [33] W. Liu, Y. Shao, Y. Zhang, Z. Chen, Wu, Y. Chen, Stefanini, L. Li, and P. Qi, "Desectbot: Design and validation of a novel two-segment decoupled continuum robotic system for endoscopic submucosal dissection," in *2024 IEEE/RSJ international conference on intelligent robots and systems*. IEEE, 2024, pp. 1–1.
- [34] C. Laschi, T. G. Thuruthel, F. Lida, R. Merzouki, and E. Falotico, "Learning-based control strategies for soft robots: Theory, achievements, and future challenges," *IEEE Control Systems Magazine*, vol. 43, no. 3, pp. 100–113, 2023.
- [35] C. Della Santina, C. Duriez, and D. Rus, "Model-based control of soft robots: A survey of the state of the art and open challenges," *IEEE Control Systems Magazine*, vol. 43, no. 3, pp. 30–65, 2023.
- [36] Z. Chen, F. Renda, A. Le Gall, L. Moccilin, M. Bernabei, T. Dangel, G. Ciuti, M. Cianchetti, and C. Stefanini, "Data-driven methods applied to soft robot modeling and control: A review," *IEEE Transactions on Automation Science and Engineering*, 2024.
- [37] M. C. Yip and D. B. Camarillo, "Model-less feedback control of continuum manipulators in constrained environments," *IEEE Transactions on Robotics*, vol. 30, no. 4, pp. 880–889, 2014.
- [38] M. Li, R. Kang, D. T. Branson, and J. S. Dai, "Model-free control for continuum robots based on an adaptive kalman filter," *IEEE/ASME Transactions on Mechatronics*, vol. 23, no. 1, pp. 286–297, 2017.
- [39] C. Della Santina, R. K. Katzschmann, A. Biechi, and D. Rus, "Dynamic control of soft robots interacting with the environment," in *2018 IEEE International Conference on Soft Robotics (RoboSoft)*. IEEE, 2018, pp. 46–53.
- [40] R. K. Katzschmann, C. Della Santina, Y. Toshimitsu, A. Biechi, and D. Rus, "Dynamic motion control of multi-segment soft robots using piecewise constant curvature matched with an augmented rigid body model," in *2019 2nd IEEE International Conference on Soft Robotics (RoboSoft)*. IEEE, 2019, pp. 454–461.
- [41] H. Jiang, Z. Wang, X. Liu, X. Chen, Y. Jin, X. You, and X. Chen, "A two-level approach for solving the inverse kinematics of an extensible soft arm considering viscoelastic behavior," in *2017 IEEE international conference on robotics and automation (ICRA)*. IEEE, 2017, pp. 6127–6133.
- [42] F. Renda, C. Armanini, V. Lebastard, F. Candelier, and F. Boyer, "A geometric variable-strain approach for static modeling of soft manipulators with tendon and fluidic actuation," *IEEE Robotics and Automation Letters*, vol. 5, no. 3, pp. 4006–4013, 2020.
- [43] C. Alessi, C. Agabiti, D. Caradonna, C. Laschi, F. Renda, and E. Falotico, "Rod models in continuum and soft robot control: a review," *arXiv preprint arXiv:2407.05886*, 2024.
- [44] C. Duriez, "Control of elastic soft robots based on real-time finite element method," in *2013 IEEE international conference on robotics and automation*. IEEE, 2013, pp. 3982–3987.
- [45] F. Largilliere, V. Verona, E. Coevoet, M. Sanz-Lopez, J. Dequidt, and C. Duriez, "Real-time control of soft-robots using asynchronous finite element modeling," in *2015 IEEE International Conference on Robotics and Automation (ICRA)*. IEEE, 2015, pp. 2550–2555.
- [46] M. Thieffry, A. Kruszewski, C. Duriez, and T.-M. Guerra, "Control design for soft robots based on reduced-order model," *IEEE Robotics and Automation Letters*, vol. 4, no. 1, pp. 25–32, 2018.
- [47] A. Melingui, J. J.-B. M. Ahanda, O. Lakhali, J. B. Mbeye, and R. Merzouki, "Adaptive algorithms for performance improvement of a class of continuum manipulators," *IEEE Transactions on Systems, Man, and Cybernetics: Systems*, vol. 48, no. 9, pp. 1531–1541, 2017.
- [48] B. Yu, J. d. G. Fernández, and T. Tan, "Probabilistic kinematic model of a robotic catheter for 3d position control," *Soft robotics*, vol. 6, no. 2, pp. 184–194, 2019.
- [49] G. Fang, X. Wang, K. Wang, K.-H. Lee, J. D. Ho, H.-C. Fu, D. K. C. Fu, and K.-W. Kwok, "Vision-based online learning kinematic control for soft robots using local gaussian process regression," *IEEE Robotics and Automation Letters*, vol. 4, no. 2, pp. 1194–1201, 2019.
- [50] J. F. Queißer, K. Neumann, M. Rolf, R. F. Reinhart, and J. J. Steil, "An active compliant control mode for interaction with a pneumatic soft robot," in *2014 IEEE/RSJ International Conference on Intelligent Robots and Systems*. IEEE, 2014, pp. 573–579.
- [51] W. Xu, J. Chen, H. Y. Lau, and H. Ren, "Data-driven methods towards learning the highly nonlinear inverse kinematics of tendon-driven surgical manipulators," *The International Journal of Medical Robotics and Computer Assisted Surgery*, vol. 13, no. 3, p. e1774, 2017.
- [52] A. Melingui, C. Escande, N. Benoudjit, R. Merzouki, and J. B. Mbeye, "Qualitative approach for forward kinematic modeling of a compact bionic handling assistant trunk," *IFAC Proceedings Volumes*, vol. 47, no. 3, pp. 9353–9358, 2014.
- [53] R. F. Reinhart, Z. Shareef, and J. J. Steil, "Hybrid analytical and data-driven modeling for feed-forward robot control," *Sensors*, vol. 17, no. 2, p. 311, 2017.
- [54] J. Zhang, X. Chen, P. Stegagno, M. Zhou, and C. Yuan, "Learning-based tracking control of soft robots," *IEEE Robotics and Automation Letters*, vol. 8, no. 10, pp. 6155–6162, 2023.
- [55] D. Braganza, D. M. Dawson, I. D. Walker, and N. Nath, "A neural network controller for continuum robots," *IEEE transactions on robotics*, vol. 23, no. 6, pp. 1270–1277, 2007.
- [56] A. Melingui, O. Lakhali, B. Daachi, J. B. Mbeye, and R. Merzouki, "Adaptive neural network control of a compact bionic handling arm," *IEEE/ASME Transactions on Mechatronics*, vol. 20, no. 6, pp. 2862–2875, 2015.
- [57] Z. Chen, X. Ren, M. Bernabei, V. Mainardi, G. Ciuti, and C. Stefanini, "A hybrid adaptive controller for soft robot interchangeability," *IEEE Robotics and Automation Letters*, vol. 9, no. 1, pp. 875–882, 2023.
- [58] T. G. Thuruthel, E. Falotico, F. Renda, and C. Laschi, "Learning dynamic models for open loop predictive control of soft robotic manipulators," *Bioinspiration & biomimetics*, vol. 12, no. 6, p. 066003, 2017.
- [59] X. Qi, Y. Mei, D. Chen, Z. Li, and X. Tan, "Design and nonlinear modeling of a modular cable-driven soft robotic arm," *IEEE/ASME Transactions on Mechatronics*, 2024.
- [60] A. Ataka, P. Qi, A. Shiva, A. Shafti, H. Wurdemann, H. Liu, and K. Althoefer, "Real-time pose estimation and obstacle avoidance for multi-segment continuum manipulator in dynamic environments," in *2016 IEEE/RSJ International Conference on Intelligent Robots and Systems (IROS)*. IEEE, 2016, pp. 2827–2832.

- [61] J. Hughes, F. Stella, C. D. Santina, and D. Rus, "Sensing soft robot shape using imus: An experimental investigation," in *Experimental Robotics: The 17th International Symposium*. Springer, 2021, pp. 543–552.
- [62] G. Gerboni, A. Diodato, G. Ciuti, M. Cianchetti, and A. Menciassi, "Feedback control of soft robot actuators via commercial flex bend sensors," *IEEE/ASME Transactions on Mechatronics*, vol. 22, no. 4, pp. 1881–1888, 2017.
- [63] C. Della Santina, A. Bicchi, and D. Rus, "On an improved state parametrization for soft robots with piecewise constant curvature and its use in model based control," *IEEE Robotics and Automation Letters*, vol. 5, no. 2, pp. 1001–1008, 2020.
- [64] A. Paszke, S. Gross, F. Massa, A. Lerer, J. Bradbury, G. Chanan, T. Killeen, Z. Lin, N. Gimelshein, L. Antiga *et al.*, "Pytorch: An imperative style, high-performance deep learning library," *Advances in neural information processing systems*, vol. 32, 2019.



Arianna Menciassi (Fellow, IEEE) received the M.Sc. degree in physics from the University of Pisa, Pisa, Italy, in 1995, and the Ph.D. degree in bioengineering from Scuola Superiore Sant'Anna (SSSA), Pisa, Italy, in 1999.

She is currently a Professor of bioengineering and biomedical robotics with SSSA, where she is the Team Leader of the Surgical Robotics & Allied Technologies area within The BioRobotics Institute. Since 2018, she has been the Coordinator of the Ph.D. in BioRobotics, and in 2019, she was also appointed as the Vice-Rector of the SSSA. Her research interests include surgical robotics, microrobotics for biomedical applications, biomechatronic artificial organs, and smart and soft solutions for biomedical devices. She pays special attention to the combination of traditional robotics, targeted therapy, and wireless solutions for therapy (e.g., ultrasound- and magnetic-based solutions).

Prof. Menciassi is an Editor for the IEEE TRANSACTIONS ON ROBOTICS and APL Bioengineering and an Associate Editor for Soft Robotics.



Zixi Chen received the M.Sc. degree in Control Systems from Imperial College in 2021. He is currently pursuing the Ph.D. degree in Biorobotics from Scuola Superiore Sant'Anna of Pisa.

His research interest includes optical tactile sensors and soft robot control with neural networks.



Qinghua Guan received the M.Sc. degree in 2017 and Ph.D degree in 2023. He is currently Postdoc researcher in Create Lab from EPFL. His research interest includes smart/architected materials, soft robotics and morphing structures.



Josie Hughes is an Assistant Professor at EPFL where she established the CREATE Lab in the Institute of Mechanical Engineering in 2021. She undertook her undergraduate, masters and PhD studies at the University of Cambridge, joining the Bio-inspired Robotics Lab (BIRL). Her PhD focused on examining the role of passivity in bio-inspired manipulators, and methodologies for exploiting morphology soft large area soft sensing. Following this, she worked as a postdoctoral associate at the Computer Science and Artificial Intelligence Laboratory,

Massachusetts Institute of Technology in USA in the Distributed Robotics Lab.

Her research focuses on developing novel design paradigms for designing robot structures that exploit their physicality and interactions with the environment. This includes the development of robotic hands, soft manipulators and automation systems for applications focused on sustainability and science. Her group explore applications for agri-food, human collaboration, robot scientists and also environmental monitoring. Her work has been published in journals including Science Robotics and Nature Machine Intelligence, and she has won numerous International Robotics Competitions Awards.



Cesare Stefanini (Member, IEEE) received the M.Sc. degree in mechanical engineering and the Ph.D. degree in microengineering, both with honors, from Scuola Superiore Sant'Anna (SSSA), Pisa, Italy, in 1997 and 2002, respectively.

He is currently Professor and Director of the BioRobotics Institute in the same University where he is also the Head of the Creative Engineering Lab. His research activity is applied to different fields, including underwater robotics, bioinspired systems, biomechatronics, and micromechatronics for medical and industrial applications. He received international recognitions for the development of novel actuators for microrobots and he has been visiting Researcher with the University of Stanford, Center for Design Research and the Director of the Healthcare Engineering Innovation Center, Khalifa University, Abu Dhabi, UAE.

Prof. Stefanini is the recipient of the "Intuitive Surgical Research Award." He is the author or coauthor of more than 200 articles on refereed international journals and on international conferences proceedings. He is the inventor of 15 international patents, nine of which industrially exploited by international companies. He is a member of the Academy of Scientists of the UAE and of the IEEE Societies RAS (Robotics and Automation) and EMBS (Engineering in Medicine and Biology).